Taylor & Francis
Taylor & Francis Group

Check for updates

Seafloor topography of Huangyan seamount chain based on GA-BP algorithm from ship survey and gravity anomaly data

Fan Zhang[a], Shuanggen Jin[a,b,c] (ID), and Charafa El Rhadiouini[a]

[a]School of Remote Sensing and Geomatics Engineering, Nanjing University of Information Science and Technology, Nanjing, China; [b]School of Surveying and Land Information Engineering, Henan Polytechnic University, Jiaozuo, China; [c]Shanghai Astronomical Observatory, Chinese Academy of Sciences, Shanghai, China

ABSTRACT

Seabed topography is important for marine geophysics and geodesy. However, conventional seabed topography inversion methods based on gravity data are constrained to a linear fitting, neglecting the impact of nonlinear terms. In this paper, we propose an innovative method for seabed topography inversion by establishing fresh mathematical relationships through machine learning techniques based on the Smith and Sandwell (SAS) method. Utilizing global sea depth data from the National Geophysical Data Center (NGDC) and gravity anomaly data from satellite altimetry, our study employs the SAS method for seabed topography inversion. The improved SAS method, enhanced by the Genetic Algorithm-Backpropagation (GA-BP) algorithm, is specifically applied to invert the Huangyan Seamount Chain topography in the South China Sea. The accuracy is evaluated by seabed topography models, including EOTPO1, GEBCO-2023, and S & S V19.1. The results show the GA-BP method significantly reduces residuals and improves the accuracy estimated by the SAS inversion method. The Root Mean Square Error (RMSE) and Mean Absolute Error (MAE) are decreased by 14.98% and 5.07%, respectively. The proposed method has valuable reference significance for future marine exploration endeavours around the world.

Introduction

Marine surveying and mapping play a pivotal role in marine exploitation and economies development worldwide. A fundamental aspect of marine surveying and mapping is to obtain the global high accuracy seabed topographic map through seabed topographic surveys. However, traditional surveying methods have disadvantages such as time-consuming, inefficiency,

and limited coverage. Satellite altimetry data can quickly and efficiently acquire global gravity data. Therefore, using satellite altimetry data to invert seafloor topography can effectively compensate the shortcomings of traditional surveying methods. The utilization of satellite altimetry in seabed topography inversion was initially proposed by Siement in the nineteenth century with postulating a relationship between spatial gravity anomalies and the seabed topography of a specific band. However, it was not used until a century later that Dixon et al. validated the feasibility of this assumption (Dixon et al., 1983). In 1983, Parker introduced gravitational potential into the frequency domain and presented the expression for gravity anomalies induced by underground material interface fluctuations in the frequency domain (Parker, 1973). In 1991, Calamant and Baudry (1991) employed Seasat, Geos-3, and Geosat altimetry geoid data and applied two-dimensional inversion technology in frequency and an iterative approach to address high-order terms of seafloor topography and geoid, which reduced the error impact of lithospheric flexural strength. Nevertheless, this method needed more integration of ship-measured sea depth data with satellite altimetry data.

Smith and Sandwell (1994) introduced a novel technique based on Watts' three-plate theoretical model (Watts, 1979) and Parker's formula. This approach utilized Geosat GM data, avoiding structural compensation assumptions, and estimated seabed topography based on the functional relationship between seabed topography and gravity anomalies in the sea area. Sandwell and Smith (1997) adopted a similar method to construct a global seabed terrain model, employing Smith's method to derive a medium-long-wave seabed terrain. In 1997, Smith and Sandwell (1997) derived a digital bathymetric map of the oceans with a horizontal resolution from 1 to 12 kilometers by combining available depth data with high-resolution marine gravity information from the Geosat and ERS-1 spacecraft. Calmant et al. (2002) employed multi-source satellite altimetry to acquire geoid height data, considering regional compensation mechanisms, and used the least squares method to predict ocean depth. Kim et al. (2010) utilized both the SAS and GGM methods to invert the submarine topography of the eastern waters in Japan, conducting accuracy assessments and comparing differences with existing models. In 2011, Kim et al. (2011) leveraged vertical gravity gradient anomalies and employed nonlinear inversion techniques based on seamount models to investigate the global distribution of seamounts. Sandwell et al. (2014) studied the tectonic plates of the seabed using ocean gravity data derived from the altimetry satellites CryoSat-2 and Jason-1, suggesting that the inversion accuracy of seabed topography was significantly improved by utilizing these new satellite altimetry data. Furthermore, Liu et al. (2022) significantly improved

the accuracy of the topography in the Emperor Seamount Chain using Convolutional Neural Networks (CNN). Wang et al. (2001) estimated high-resolution seabed topography in the China Sea and adjacent seas using the admittance method with higher resolution and accuracy than the widely used ETOPO model. Ouyang et al. (2015) evaluated the accuracy of the ETOPO1 model in the South China Sea using the gravity geological method. Li and Bao (2016) analyzed the SAS method and gravity geology method in the sea area near the West Island of Japan, and Sui et al. (2017) conducted seabed topography inversion experiments in some areas of the North Pacific based on the SAS method. However, accuracy of seabed topography is still low and more improvements are still needed.

Fan et al. (2018) pioneered a linear regression analysis technology for estimating seabed topography, and later applied multiple regression technology for seabed topography inversion with yielding favourable results. Yang et al. (2018) utilized the simulated annealing method for seabed topography inversion, demonstrating the method's effectiveness in finding global optimal solutions, albeit with a slower inversion process. Fan et al. (2021) emphasized the importance with considering three-term or four-term seabed topography to maximize the information contained in sea surface gravity data and proposed a least squares collocation inversion method with considering the nonlinear term of seabed topography and highlighted the forward modeling results of one-term seabed topography as crucial to the contribution of gravity information. Sun et al. (2022) asserted that marine gravity field inversion based on satellite altimetry remained the primary technical approach for refined modeling of global seabed topography. Li et al. (2023) introduced a fully connected deep neural network (FC-DNN) to merge geometric algebra (GA), visual geometry group (VGG), and the deflection of vertical (DOV) to predict the bathymetry in the South China Sea. The optimized ensemble model of machine learning techniques was applied to the residual gravity anomalies to estimate bathymetry by the gravity–geologic method (GGM) from various geospatial information, including shipborne depth, shipborne gravity anomalies, and satellite altimetry-derived free-air gravity anomalies in the Ulleung Basin in the East Sea (Kim et al., 2023).

They underscored the need to explore the application of artificial intelligence technology in refined seabed topography modeling. However, conventional seabed topography inversion methods based on gravity data are constrained to a linear fitting, simply considering the impact of nonlinear terms or even neglecting it. In this paper, we propose an innovative method for seabed topography inversion by establishing fresh mathematical relationships through machine learning techniques based on the Smith and Sandwell (SAS) method. In Section 2, study area and data are introduced,

methods are given in Section 3, results and analysis are presented in Section 4, and finally conclusions are given in Section 5.

Study Area and Data

The study focuses on the Huangyan seamount chain, located in the southeast of the Zhongsha Islands within the coordinates of 14°-16°N and 116°-118°30'E. The chain includes Huangyan Island, the sole island in the Zhongsha Islands with rocks protruding above the water, situated approximately 160 nautical miles away from the Zhongsha Atoll. The island's reef rim forms an irregular, large 'C' shape, spanning 55 km in length and covering an area of 150 km². The study area's latitude and longitude are extended outward by 30 to account for edge effects, as illustrated in Figure 1.

Shipborne Sounding Data

Figure 2 displays the distribution of control points within the study area. The shipborne-sounding data utilized in this paper originates from measurements released by the United States National Geophysical Data Center (NGDC). The single-beam data spans 42 years (1961–2002), while the
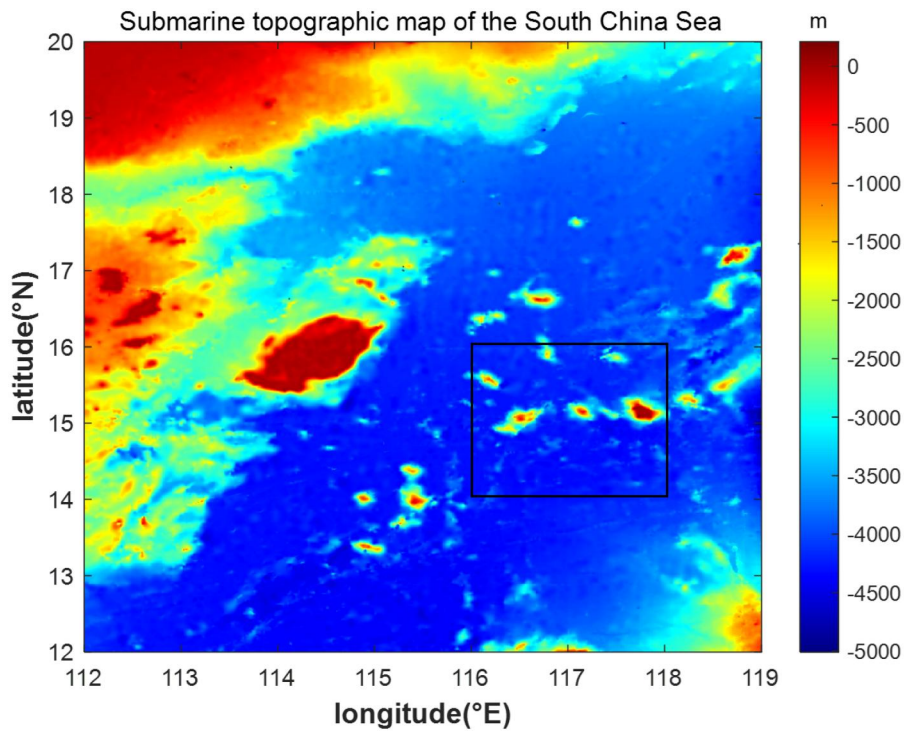

Figure 1. Schematic map of the study area.

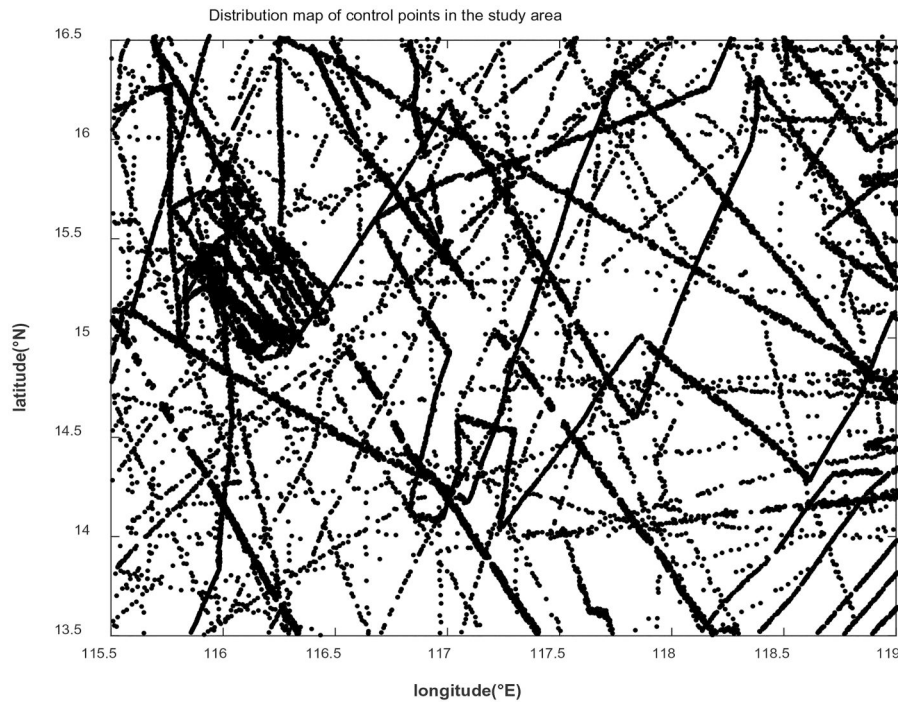Distribution map of control points in the study area

Figure 2. Study area control point distribution map.

multi-beam data spans 16 years (2004–2019). To ensure data accuracy, the global topographic model GEBCO is a constraint for mutual difference comparison. Employing the triple mean square error criterion, we eliminate gross error points in the single-beam data, resulting in 24,381 single-beam ship measurement points. To validate the accuracy of the model in this paper, the latest GEBCO-2023, ETOPO1, and S&S V19.1 models are used for verification. GEBCO-2023 and S&S V19.1 are internationally recognized high-precision terrains, incorporating data from single-beam and multi-beam surveys, as well as altimetry-inverted topography, representing high-quality data sources. ETOPO1, released in 2009 as the last edition in its series, is used as an additional reference for precision comparison.

Gravity and Validation Data

Gravity anomaly data are sourced from Smith and Sandwell at the Scripps Institution of Oceanography (SIO) at the University of California, San Diego (UCSD). They are based on Version 29.1, with a resolution of $1' \times 1'$. The validation data employed in this study include GEBCO-2023, ETOPO1, and S & S V19.1. The map of gravity anomalies in the study area is depicted in Figure 3.
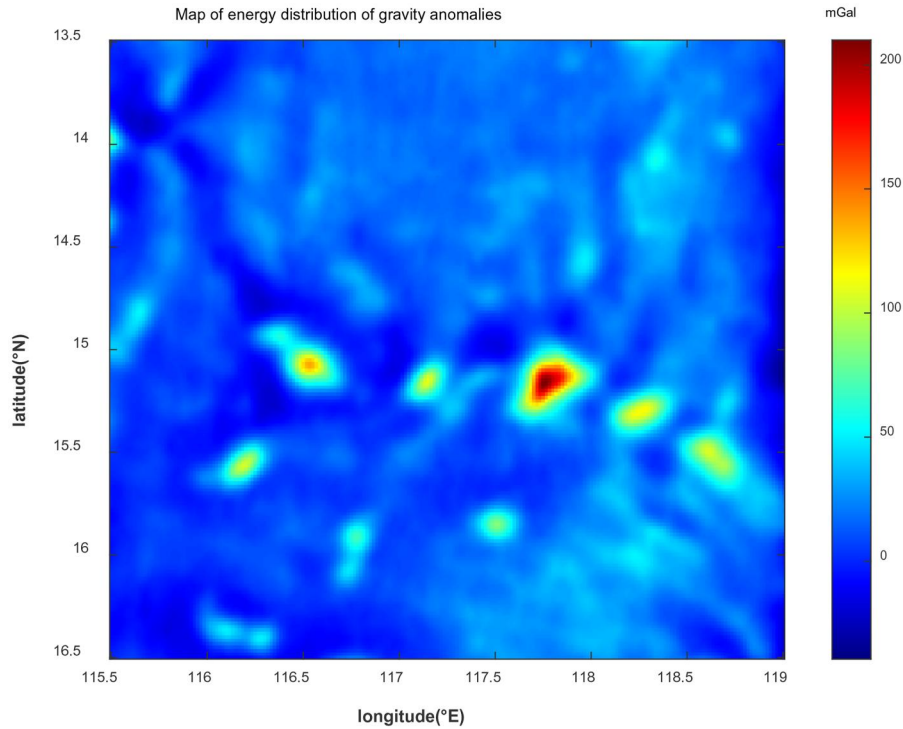
Figure 3. Map of gravity anomalies in the study area.

Methods

Inversion Methods

The application of response function and coherence analysis, grounded in admittance function theory, highlights a robust correlation between gravity anomalies and ship measurements in the mid-wave. The 'remove-restore' method is employed to categorize the inversion band into long wave, medium wave, and short wave. In the spatial domain, linear fitting is executed using the residual sea depth and medium wave gravity anomaly, facilitating terrain inversion through an idealized scale factor under the linear relationship (Smith and Sandwell, 1994).

Since gravity anomalies and seafloor topography exhibit high correlation within a specific band, Smith and Sandwell defined the seabed topography model as the sum of the band-pass filter value of 15–160 km and the depth of the long wave part $d_{lp}(x)$.

$$depth = d_l p(x) + S(x)g(x) \tag{1}$$

where the band-pass filtering value is the product of the gravity anomaly g(x) and the scaling factor S(x) after band-pass filtering and downward continuation. The satellite altimetry gravity anomaly in the frequency domain $(G_0(k))$ is extended downward to the average sea depth through

initial band-pass filtering:

$$G(k) = G_0(k)W(k)exp(2\pi kd) \qquad (2)$$

where G(k) is the gravity field after band-pass filtering and downward continuation. The initial value of the gridded ship-measured water depth data in the frequency domain is denoted as $B_0(k)$, calculated using bandpass filtering:

$$H(k) = B_0(k)W(k) \qquad (3)$$

where H(k) represents seabed terrain, and B(k) is processed by low-pass filtering:

$$D_{lp}(k) = B_0(k)\left[1 - W_1(k)\right] \qquad (4)$$

In this study, the band-pass filter's wavelength is set to 20–200 km, and the scale factor is determined by Equations (2) and (3). The classical method is obtained using a robust linear regression technique, while the improved method establishes a new mathematical relationship directly through a machine learning method. Seabed topography with a wavelength less than 20 km is acquired using ship-measured water depth data, and the residual bathymetry is gridded.

The neural network exhibits nonlinear information processing capabilities. By learning from input training data, the synaptic weight values are adjusted to meet the environmental requirements of the training data, providing predictive and control abilities for samples not partaking in the training. The long-term and short-term memory networks, a variant of the recurrent neural network, effectively address the problem of gradient disappearance in traditional model training. An inversion method utilizing GA-BP to estimate seabed topography is proposed to establish an accurate mathematical relationship. The GA-BP network is tested, optimized, and adjusted using ship survey data and gravity anomalies as prior knowledge.

Back-Propagation Neural Network (BPNN) (Guo et al., 2024), a widely used intelligence algorithm, is employed for modeling, predicting, abstracting, and simulating biological neural networks. Mimicking the human brain's problem-solving approach, BPNN discovers correlations between data effectively. The strong correlation between gravity data and water depth data in this study, as depicted in Figure 4, is justified by using BPNN for model construction and inversion. The model construction principle is shown in Figure 5.

In the process of BPNN training, it is easy to fall into the local minimum value, so the genetic algorithm is introduced to optimize it. Genetic algorithms are inspired by the powerful adaptive capacity of organisms in their natural environment. By simulating and abstracting the biological evolution
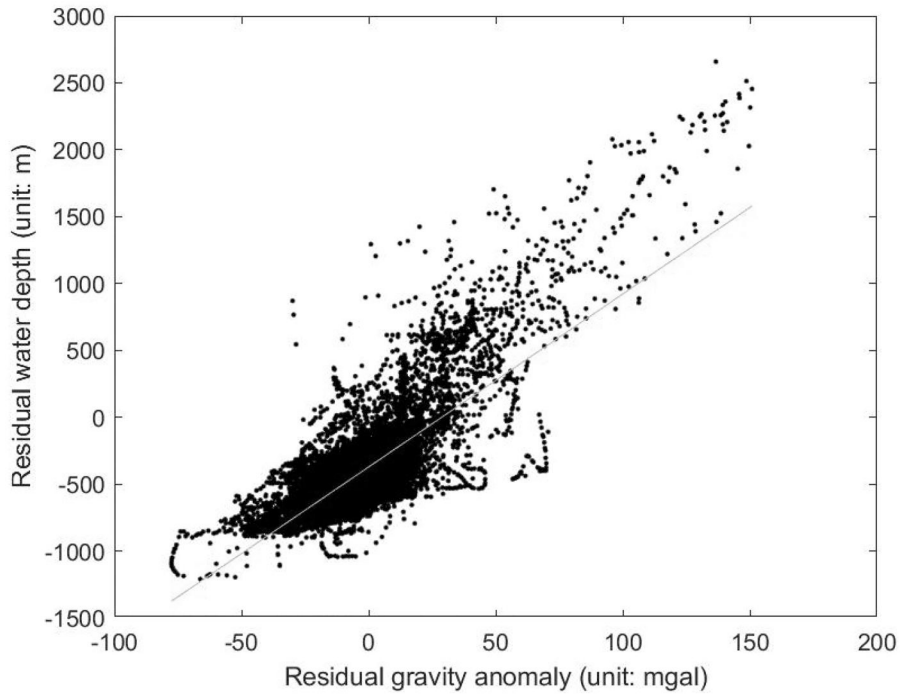
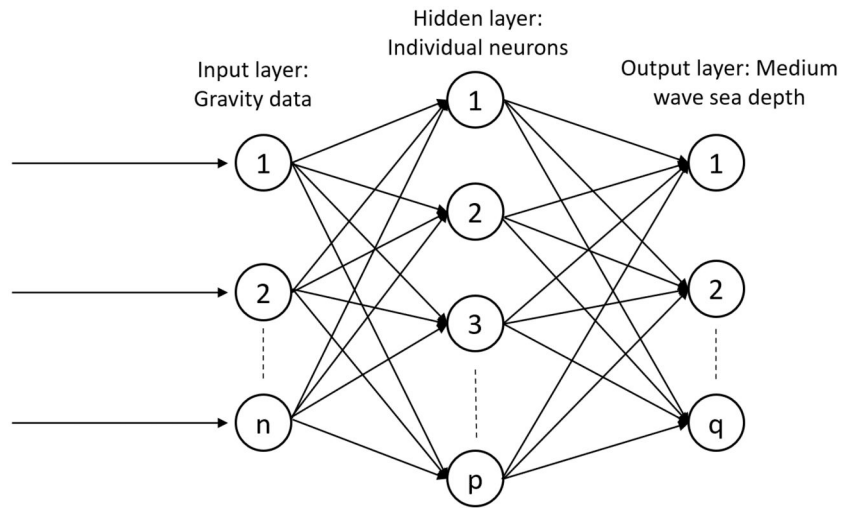**Figure 4.** Plots of gravity anomalies and bathymetric scatters.

Figure 5. BPNN model presentation.

process, the genetic algorithm based on the evolution of natural biological evolution is constructed. A genetic algorithm includes the main steps of natural organisms in the evolution process, namely, selection, mutation, and crossover, corresponding to the three operators in the genetic algorithm. Under the specific optimization problem, the genetic algorithm will

generate a feasible solution to multiple problems as a population, and then let the population perform operations including selection, mutation, crossover and others in the simulation of biological evolution. After a certain number of population reproductions (iterations), by calculating the fitness of the population, the optimal individual in the final population is found, which represents the approximate optimal solution of the optimization problem. The two algorithms have obvious complementary advantages, so this paper uses the fusion method of the two algorithms to improve the performance of the algorithm and the accuracy of the model. The algorithm flow is shown in Figure 6. In the GA-BP neural network, the genetic algorithm is used for global searching of the optimal network weights and thresholds, while the BP algorithm is used for local fine-tuning of these parameters. Specifically, the genetic algorithm first optimizes the initial weights and thresholds of the neural network through selection, crossover, and mutation operations to generate a series of solutions (i.e. network parameters). Then, the best-performing solutions are selected as the starting
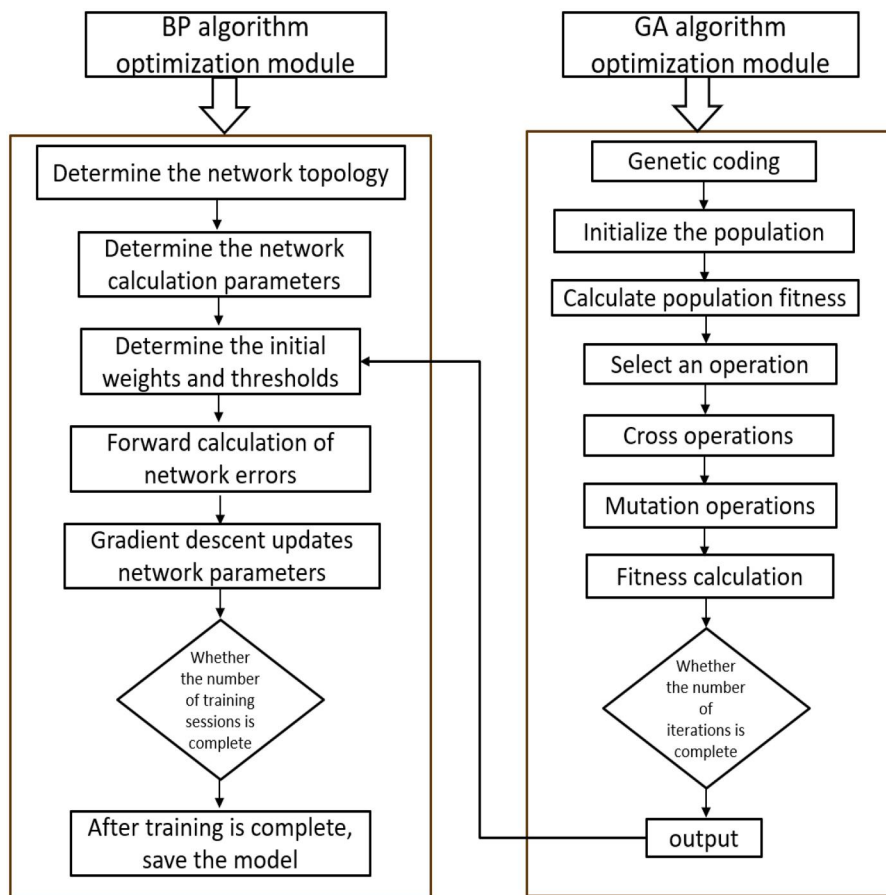

Figure 6. GA-BP model building flowchart.

point for the BP algorithm, which quickly makes local adjustments. By combining these methods, the efficiency and accuracy of neural network training can be improved, especially in solving complex nonlinear problems (Kim et al., 2023).

Seabed Topographic Inversion Process

The SAS method, renowned for its robustness and versatility, is employed to invert the seabed topography within the wavelength range of 10–120 km (Figure 7). This sophisticated method categorizes the model into long wave ($>$ 200 km), medium wave (20 km), and short wave ($<$ 20 km) using the 'remove-restore' program. The calculation steps involve meticulous data processing and transformation:

a. The ship-measured water depth data is meticulously gridded to generate a precise 1' $\times$ 1' grid water depth model, ensuring high-resolution representation.

b. The grid water depth model data is seamlessly introduced into the frequency domain, facilitating the derivation of the long-wave sea depth model through low-pass filtering (200 km) using the Fourier transform, ensuring accurate representation of the long-wave features.

c. The interpolation of the long-wave sea depth component of the ship measuring point, coupled with the derivation of the residual sea depth, ensures the meticulous representation of the seabed topography, capturing intricate details with precision.

d. The processing of the gravity anomaly by Fourier transform, followed by band-pass filtering and downward continuation ($20 \sim 200$ km), ensures the accurate derivation of the gravity anomaly in the inversion band, crucial for precise seabed topography estimation.

e. The division of the residual sea depth and gravity anomaly components of the ship measuring point into training and testing data, meticulously input into the GA-BP network, ensures the optimization of the training results to obtain the optimal network, guaranteeing the accuracy and reliability of the inversion process.

f. The conversion of the gravity anomaly in the inversion band into scatter points, input into the debugged GA-BP network, ensures the meticulous derivation of the inversion band sea depth model, capturing intricate details with precision.

g. The meticulous superimposition of the long-wave seabed model and the inversion band seabed model, followed by external verification, ensures the accuracy and reliability of the inversion seabed topographic model, providing a comprehensive representation of the seabed topography.
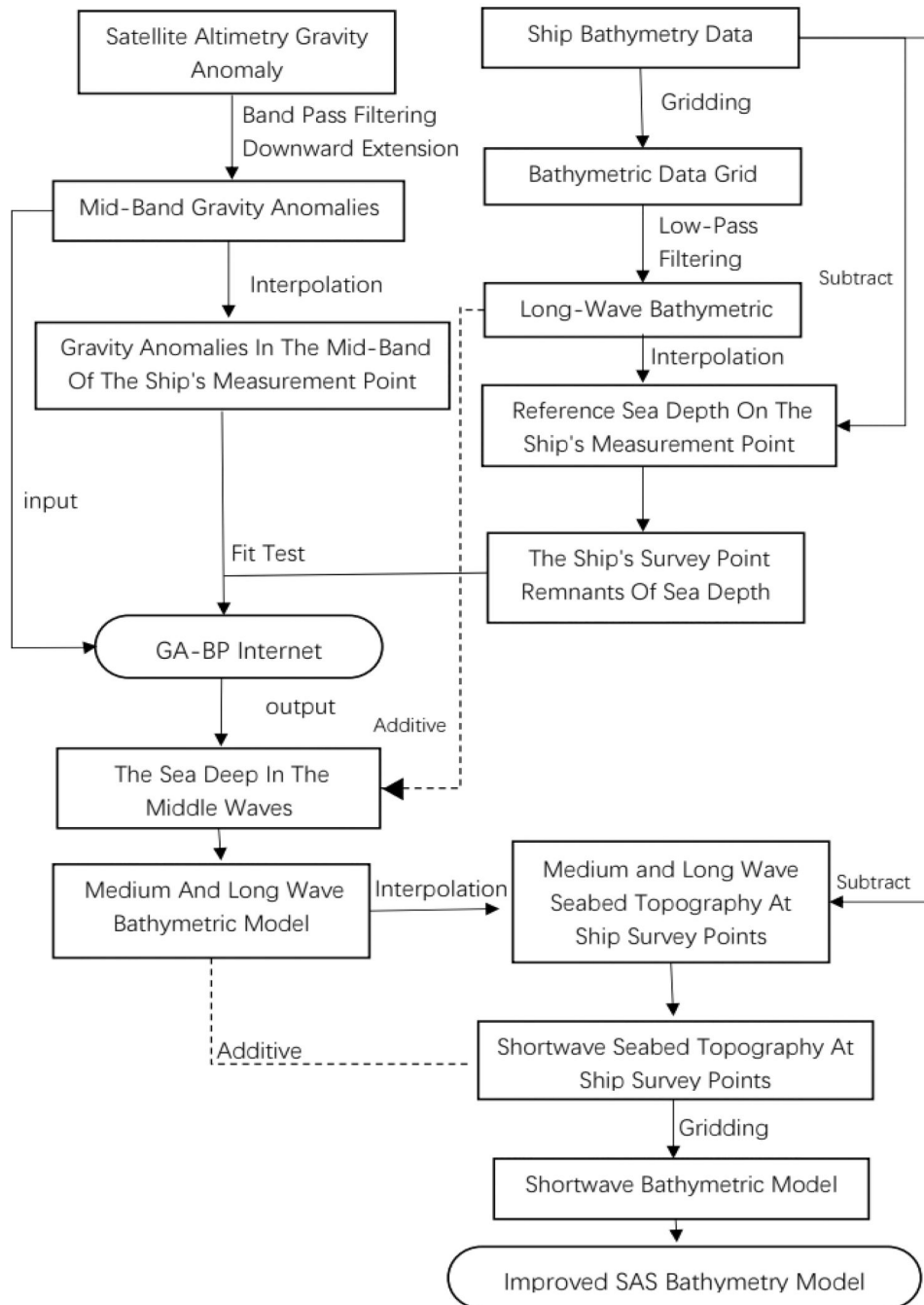
Figure 7. Flowchart of seabed topography inversion.

Results and Analysis

Precision Analysis

Here accuracy analysis is conducted using check points that are not involved in the inversion calculation. Figure 8 illustrates the residuals

obtained from the inversion of the mathematical relationship between the ETOPO1 model and the least squares proportional factor and GA-BP estimation. Significant differences in the fitting of mathematical relationships established by different methods are observed. The GA-BP residual distribution outperforms the least squares method. Statistical parameters are presented in Table 1, where the residual sum of squares represents the effect of random errors.

In the statistical analysis of the three models, it's evident that EOTPO1 has poor accuracy due to its early release time. The SAS method, utilizing the least squares method for linear inversion, struggles to constrain undulating terrains like mountains and valleys adequately. The lack of a nonlinear relationship in the inversion process leads to poor results for topographic data. This paper proposes using the GA-BP inversion method, which employs a nonlinear relationship, resulting in more detailed and accurate terrain inversion, especially in areas with significant relief.

Topography Comparison

ETOPO1, S&S V19.1, GEBCO-2023, SAS, and the GA-BP network established topography in this paper are compared and analyzed for accuracy,
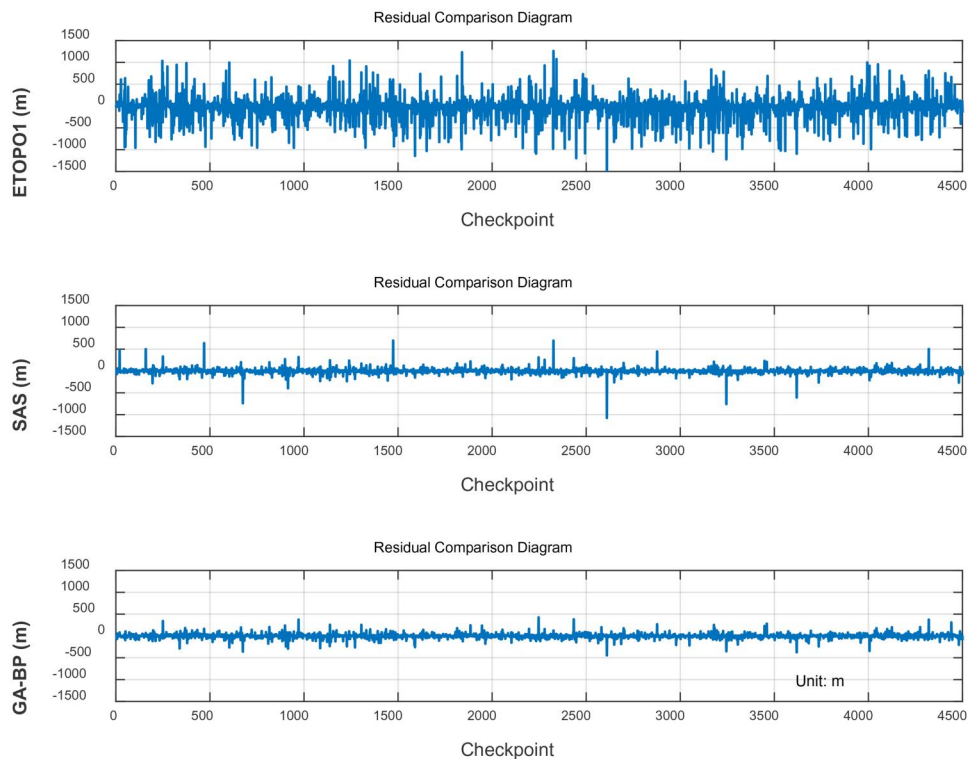

Figure 8. Comparison chart of residuals.

Table 1. Residual analysis table(m).

DATA	SSE	RMSE	MAE	R
EOTPO1	2.06×10^7	204.55	101.07	0.78
SAS	1.19×10^7	49.13	21.29	0.98
GA-BP	8.60×10^6	41.77	20.21	0.99

Notes: SSE is the sum of squares of errors, RMSE is the root mean square error, MAE is the mean absolute error, and R is the coefficient of determination

Table 2. Statistical parameters of different seabed topographic models(m).

DATA	MAX	MIN	MEAN	STD	CORRELATION
GA-BP	30.67	−4577.11	−3985.90	274.21	1.0000
EOTPO1	67.00	−4855.00	−3986.14	286.64	0.9489
SAS	481.36	−4629.35	−3991.99	245.39	0.9803
GEBCO-2023	−3.00	−4538.00	−4004.20	240.56	0.9936
S&S V19.1	120.00	−4596.00	−3977.28	265.83	0.9893

Notes: MAX is the maximum value of the depth, MIN is the minimum value, MEAN is the average value, and STD is the standard deviation

respectively. The data from different seabed terrain models is statistically analyzed, as shown in Table 2. The average water depth difference between the seabed terrain model estimated by machine learning, the V19.1 model, and the GEBCO-2023 model is insignificant. The sea area of Huangyan Island has been China's inherent territory since ancient times. In addition to the hundreds of extensive reefs in the form of belt rings in the waters of Huangyan Island, the rest are generally underwater by 0.5–3 m. The highest elevation of the reef blocks is about 1.8 m. Therefore, from the maximum value, the GA-BP estimation model and the GEBCO-2023 model are closer to the actual terrain. The correlation coefficients of the GA-BP model with the ETOPO1 model, SAS model, GEBCO-2023 model, and V19.1 model are 0.9489, 0.9803, 0.9936, and 0.9893, respectively. It can be seen that the GA-BP model is the closest to the international high-precision seabed topography GEBCO-2023 model.

The reef rim of Huangyan Island is 55 km long and covers an area of 150 km^2, showing an irregular large ' C ' shape. The comparison between Figure 9 and Figure 10 shows that the GA-BP estimation model is closer to the actual terrain than the linear inversion model of least squares regression in the near sea level part. The reason is that the linear inversion ignores the nonlinear term and cannot effectively constrain the medium wave sea depth terrain. As a result, the inversion results do not match the actual topography in the peaks or deep valleys of the rugged terrain.

In order to further analyze the accuracy of the model, the checkpoints without being involved in the inversion process are used to obtain the corresponding sounding data by interpolating each model, and the model's accuracy is compared by subtracting the checkpoints. The different statistical results of different terrain models at checkpoints are given in Table 3. At each monitoring point, each model's average sea depth difference is
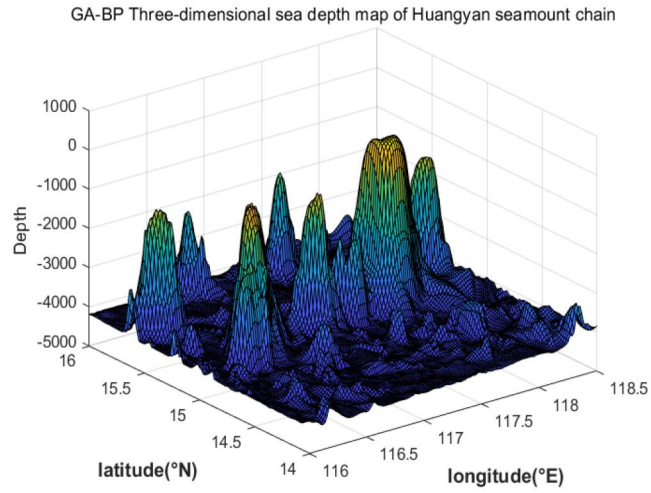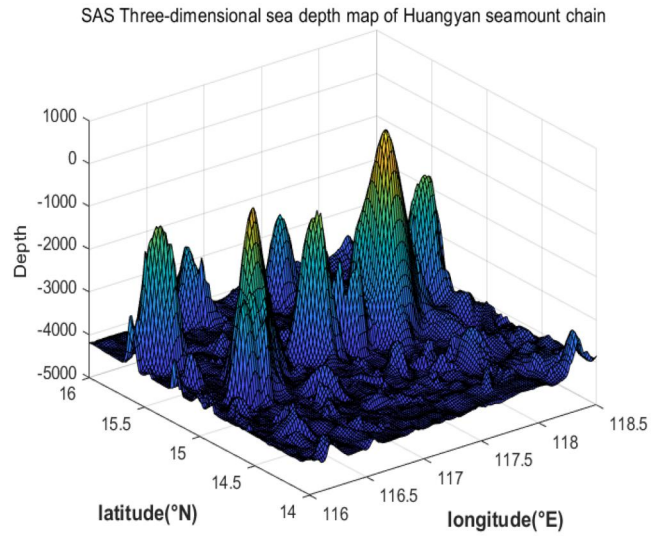
Figure 9. GA-BP 3D sea depth map.

Figure 10. SAS 3D sea map.

Table 3. Statistics on the difference between the check points data and different seabed topography models(m).

DATA	MAX	MIN	MEAN	STD	CORRELATION
GA-BP	426.01	−445.81	−0.80	41.77	0.9946
EOTPO1	1261.79	−1665.82	−19.43	203.64	0.8868
SAS	696.19	−1075.23	−0.91	49.13	0.9925
GEBCO-2023	254.65	−679.4	−0.12	45.26	0.9939
S&S V19.1	411.59	−769.57	0.84	38.33	0.9953

Notes: MAX is the maximum value of the error, MIN is the minimum value, MEAN is the average value, and STD is the standard deviation, CORRELATION is the correlation between the true value and the measured value at the verification point
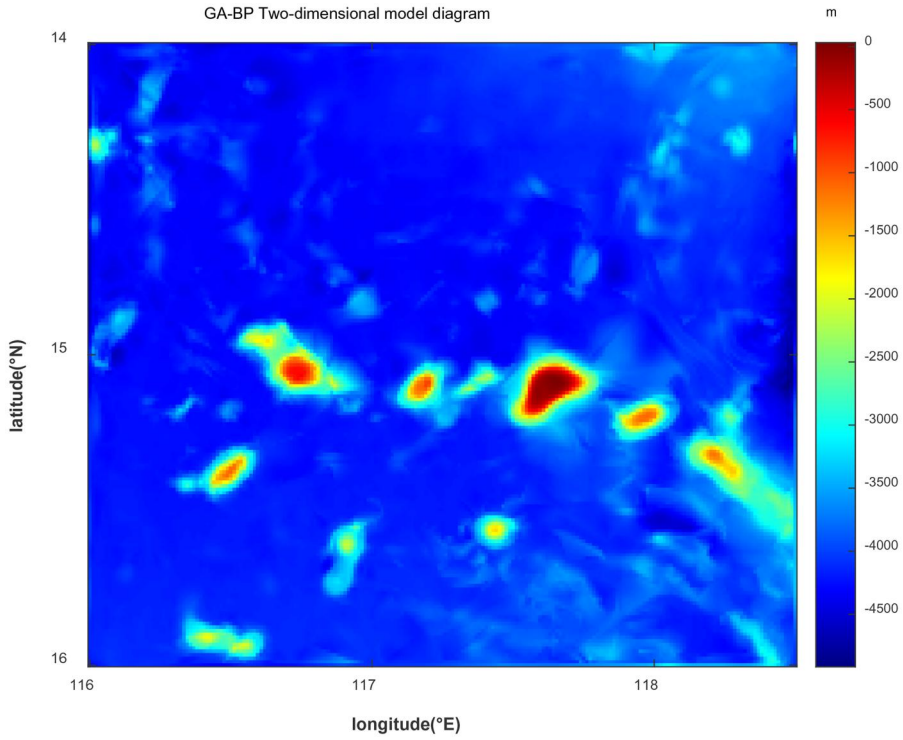
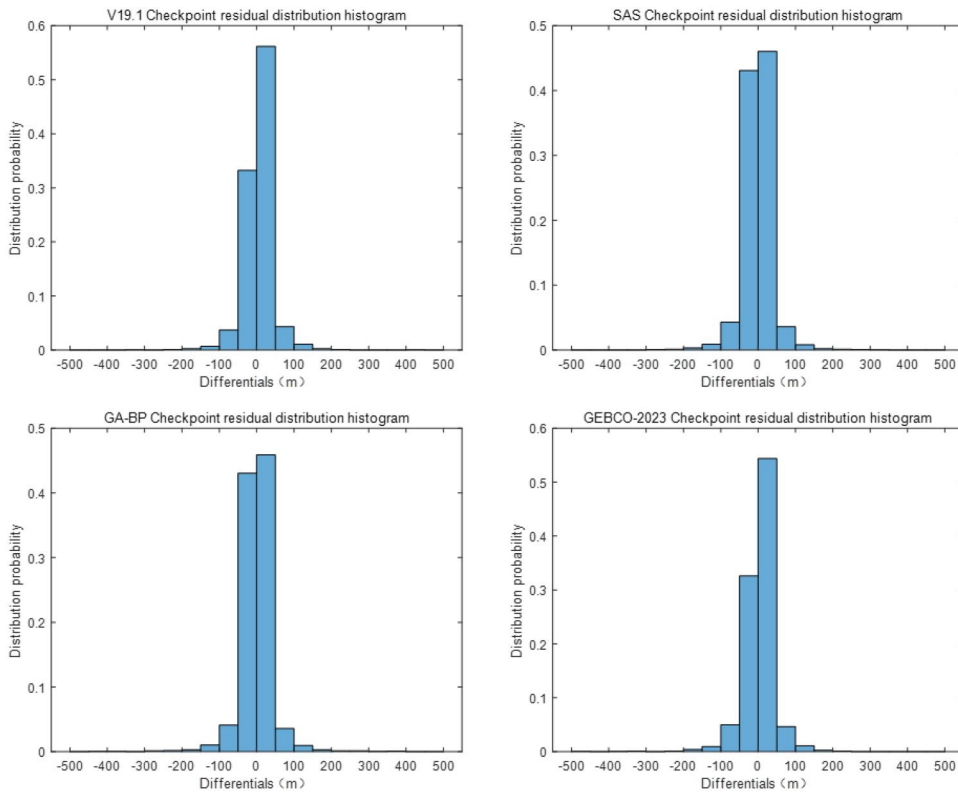**Figure 11.** GA-BP model 2D diagram.

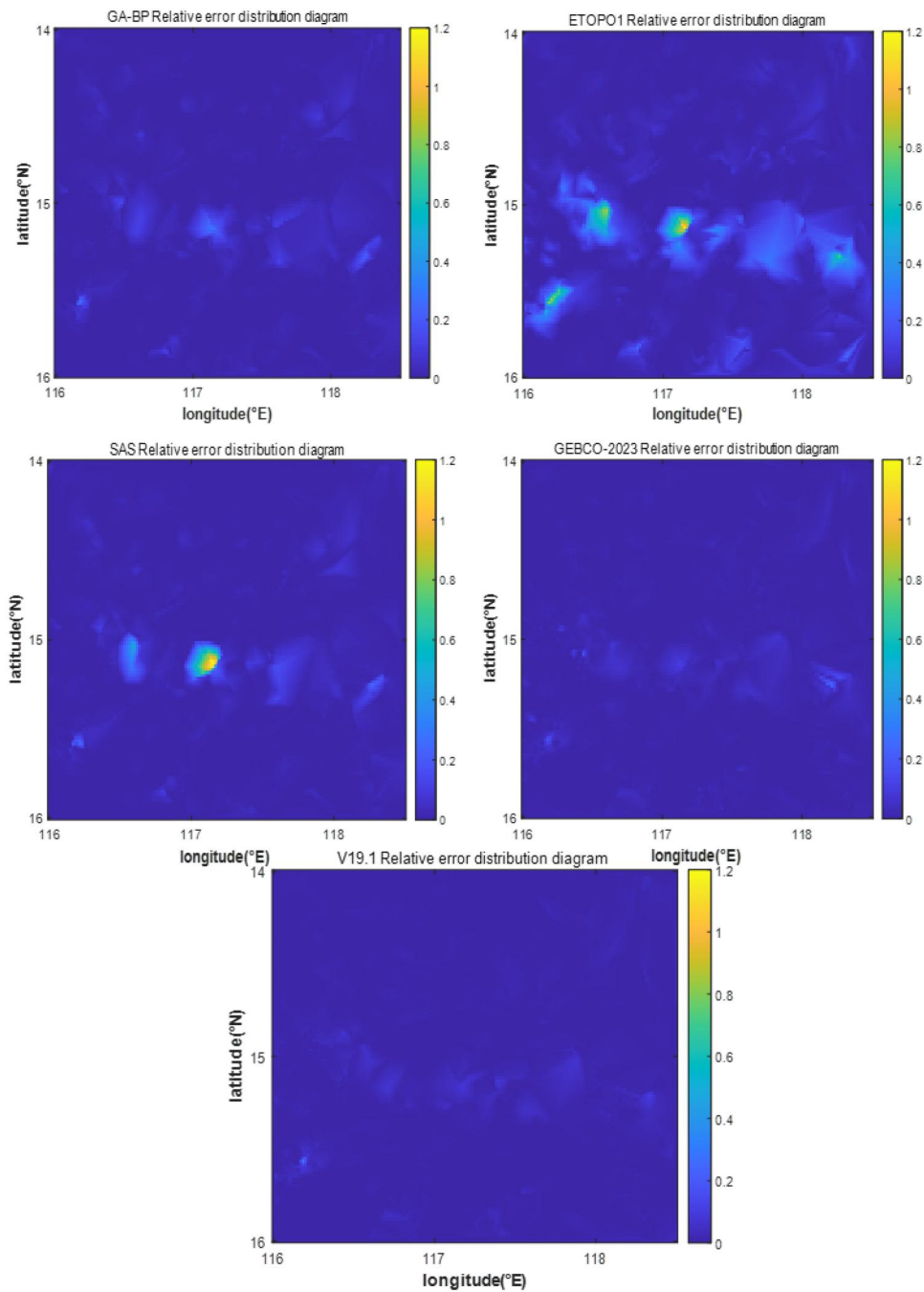**Figure 12.** Sea depth difference statistical histogram.

Figure 13. Relative error distribution plot of different models.

close. However, the difference between the maximum and minimum values of the ETOPO1 model is significant, and the statistical parameters show that the ETOPO1 model's accuracy is lower than other models. According

Table 4. Table of relative error statistics for different models(m).

DATA	MAX	MIN	MEAN	STD
GA–BP	0.2998	−0.0317	0.0114	0.0048
EOTPO1	1.1451	−0.1244	0.0390	0.0421
SAS	1.3130	−0.0275	0.0156	0.04448
GEBCO-2023	0.2339	−0.0513	0.0081	0.0053
S&S V19.1	0.2685	−0.1155	0.0068	0.0042

Notes: MAX is the maximum relative error, MIN is the minimum value, MEAN is the average value, and STD is the standard deviation

to the standard deviation statistics, the residual standard deviations of the GA-BP model and ETOPO1, SAS, GEBCO-2023, and V19.1 models are 41.77, 203.64, 49.13 and 45.26 m, 38.33 m, respectively. The residual statistics show that the accuracy of the GA-BP model is higher than that of the ETOPO1 model and is comparable to the high-precision V19.1 model and the GEBCO-2023 model (Figure 11).

Error Statistics

Figure 12 shows the histogram of the distribution of sea depth differences from different models. The sea depth difference (<50 m) is 88.92% for the GA-BP model as well as 62.51%, 86.99%, and 89.39% for the ETOPO1, GEBCO-2023 and V19.1 models. Moreover, the sea depth difference (<100 m) is 96.63% for the GA-BP model as well as 96.65% and 97.44% for the GEBCO-2023 and V19.1 models, respectively.

As shown in Figure 13, the relative error distribution has prominent spatial distribution characteristics. The relative error distribution is more significant in the seamount and valley areas and minor in the gentle terrain area. The maximum relative error of the GA-BP model in this paper is 0.2998, which is higher than the terrain model of ETOPO1 and least squares inversion. The standard deviation (STD) is 0.0048, second only to the V19.1 model. From the perspective of relative error, the accuracy of the GA-BP model in this paper is equivalent to that of the V19.1 model and GEBCO-2023 model and higher than that of the ETOPO1 model.

As shown in Table 4, from the relative error analysis, using the SAS method improved by the GA-BP algorithm effectively reduces the inversion error in areas with rugged terrain and solves the problem of overfitting caused by ignoring nonlinear terms in traditional methods. The accuracy of seabed topography inversion by the GA-BP model is close to that of the international advanced V19.1 model and GEBCO-2023 model.

Conclusion

This paper proposed a new nonlinear relationship between gravity anomaly and ship bathymetry using GA-BP. The estimation results are validated and

compared with international high-precision terrain models, including the V19.1 model, GEBCO-2023 model, and ETOPO1 model. External verification, accuracy assessment, and error analysis are conducted through checkpoints. Main conclusions are obtained as followings:

a. The GA-BP method significantly reduces residuals estimated by the SAS inversion method. The Root Mean Square Error (RMSE) and Mean Absolute Error (MAE) are decreased by 14.98% and 5.07%, respectively. The coefficient is increased from 0.98 to 0.99, indicating that the GA-BP method's estimation has a better fitting effect with good reliability. Additionally, the GA-BP model demonstrates higher accuracy with addressing the issue of missing nonlinear terms in traditional methods. The three-dimensional map illustrates that topographic inversion results near sea level are closer to actual topography.

b. The correlation coefficient between the GA-BP model and the EOTPO1 model is 0.9489. The correlation coefficients between the GA-BP model, the GEBCO-2023 model, and the V19.1 model reach 0.9936 and 0.9893, respectively. These results confirm that the GA-BP model's accuracy is on a par with international high-precision seabed topography models.

c. The residual standard deviation difference of the GA-BP model at the checkpoint is much smaller than that of the ETOPO1 model and traditional SAS methods. The relative error is small in flat terrain areas and extensive in seamount chains, valleys, and other challenging terrains. The nonlinear inversion of the GA-BP algorithm primarily reduces the relative error in rugged terrain.

Disclosure statement

Funding

ORCID

Shuanggen Jin (iD) http://orcid.org/0000-0002-5108-4828

References

Baudry, N., and S. Calmant. 1991. "3-D Modelling of Seamount Topography from Satellite Altimetry." *Geophysical Research Letters* 18 (6): 1143–1146. https://doi.org/10.1029/91GL01341

Calmant, S., M. Berge-Nguyen, and A. Cazenave. 2002. "Global Seafloor Topography from a Least-Squares Inversion of Altimetry-Based High-Resolution Mean Sea Surface and Shipboard Soundings." *Geophysical Journal International* 151 (3): 795–808. https://doi.org/10.1046/j.1365-246X.2002.01802.x

Dixon, T. H., M. Naraghi, M. K. McNutt, and S. M. Smith. 1983. "Bathymetric Prediction from Seasat Altimeter Data." *Journal of Geophysical Research: Oceans* 88 (C3): 1563–1571. https://doi.org/10.1029/JC088iC03p01563

Fan, D., S. S. Li, J. J. Yang, S. Y. Meng, Z. B. Xing, C. Zhang, and J. K. Feng. 2020. "Inversion of Seafloor Topography in the Southwest Indian Ocean Using Multiple Regression Analysis." *Journal of Surveying and Mapping* 49 (2): 147–161.

Fan, D., S. S. Li, S. Y. Meng, Z. B. Xing, and X. X. Li. 2018. "Linear Regression Analysis Technique is Used to Estimate Seabed Topography." *Chinese Journal of Inertial Technology* 26 (1): 24–32. https://doi.org/10.13695/j.cnki.12-1222/o3.2018.01.005

Fan, D., S. S. Li, S. Y. Meng, Z. B. Xing, C. Zhang, J. K. Feng, and Z. H. Qu. 2021. "Analysis of the Influence of High-Order Term of Seabed Topography on Sea Surface Gravity Information." *Geomatics and Information Science of Wuhan University* 46 (9): 1328–1335. https://doi.org/10.13203/j.whugis20190192

Fan, D., S. S. Li, S. Y. Meng, Z. B. Xing, J. K. Feng, and C. Zhang. 2018. "Inversion of Seabed Topography in the Philippines Sea Area by Combining Multi-Source Gravity Data." *Journal of Surveying and Mapping* 47 (10): 1307–1315.

Fan, D., S. S. Li, Y. Z. Ouyang, S. Y. Meng, C. Chen, Z. B. Xing, and C. Zhang. 2021. "Least Square Collocation Inversion Method considering Nonlinear Term of Seabed Topography." *Journal of Surveying and Mapping* 50 (7): 953–971.

Guo, L., Y. Yuan, W. Tang, and H. Xue. 2024. "Steady-State Characteristics Prediction of Marine Towing Cable with BPNN." *Ships and Offshore Structures* 19 (2): 208–222. https://doi.org/10.1080/17445302.2022.2157138

Kim, J. W., R. R. von Frese, B. Y. Lee, D. R. Roman, and S. J. Doh. 2011. "Altimetry-Derived Gravity Predictions of Bathymetry by the Gravity-Geologic Method." *Pure and Applied Geophysics* 168 (5): 815–826. https://doi.org/10.1007/s00024-010-0170-5

Kim, K. B., J. S. Kim, and H. S. Yun. 2023. "Bathymetry Estimation Using Machine Learning in the Ulleung Basin in the East Sea." *Sensors and Materials* 35 (9): 3351–3362. https://doi.org/10.18494/SAM4415

Kim, K. B., Y. S. Hsiao, J. W. Kim, B. Y. Lee, Y. K. Kwon, and C. H. Kim. 2010. "Bathymetry Enhancement by Altimetry-Derived Gravity Anomalies in the East Sea (Sea of Japan)." *Marine Geophysical Researches* 31 (4): 285–298. https://doi.org/10.1007/s11001-010-9110-0

Li, Q. Q., and L. F. Bao. 2016. "Comparison of Methods for Altimetry Gravity Field Inversion of Seabed Topography." *Hydrographic Surveying and Charting* 36 (5): 1–4. https://doi.org/10.3969/j.issn.1671-3044.2016.05.001

Li, Q., Z. Zhai, Q. Li, L. Wu, L. Bao, and H. Sun. 2023. "Improved Bathymetry in the South China Sea from Multisource Gravity Field Elements Using Fully Connected Neural Network." *Journal of Marine Science and Engineering* 11 (7): 1345. https://doi.org/10.3390/jmse11071345

Liu, P., S. Jin, and Z. Wu. 2022. "Assessment of the Seafloor Topography Accuracy in the Emperor Seamount Chain by Ship-Based Water Depth Data and Satellite-Based Gravity Data." *Sensors (Basel, Switzerland)* 22 (9): 3189. https://doi.org/10.3390/s22093189

Ouyang, M. D., Z. M. Sun, Z. H. Zhai, and X. G. Liu. 2015. "The Seabed Terrain Model of South China Sea is Established by Using Altimetry Gravity Anomaly." *Geodesy and Geodynamics* 35 (3): 490–494. https://doi.org/10.14075/j.jgg.2015.03.030

Parker, R. L. 1973. "The Rapid Calculation of Potential Anomalies." *Geophysical Journal International* 31 (4): 447–455. https://doi.org/10.1111/j.1365-246X.1973.tb06513.x

Sandwell, D. T., and W. H. F. Smith. 1997. "Marine Gravity Anomaly from Geosat and ERS 1 Satellite Altimetry." *Journal of Geophysical Research: Solid Earth* 102 (B5): 10039–10054. https://doi.org/10.1029/96JB03223

Sandwell, D. T., R. D. Müller, W. H. Smith, E. Garcia, and R. Francis. 2014. "New Global Marine Gravity Model from CryoSat-2 and Jason-1 Reveals Buried Tectonic Structure." *Science* 346 (6205): 65–67. https://doi.org/10.1126/science.1258213

Smith, W. H., and D. T. Sandwell. 1994. "Bathymetric Prediction from Dense Satellite Altimetry and Sparse Shipboard Bathymetry." *Journal of Geophysical Research: Solid Earth* 99 (B11): 21803–21824. https://doi.org/10.1029/94JB00988

Smith, W. H., and D. T. Sandwell. 1997. "Global Sea Floor Topography from Satellite Altimetry and Ship Depth Soundings." *Science* 277 (5334): 1956–1962. https://doi.org/10.1126/science.277.5334.1956

Sui, X. H., R. L. Zhang, X. Y. Wan, and Y. Li. 2017. "Seabed Terrain Inversion and Analysis Based on Satellite Altimetry Data." *Spacecraft Engineering* 26 (3): 130–136. https://doi.org/10.3969/j.issn.1673-8748.2017.03.020

Sun, H., Q. Q. Li, L. F. Bao, Z. Y. Wu, and L. Wu. 2022. "Progress and Development Trend of Global Refined Seafloor Topography Modeling." *Geomatics and Information Science of Wuhan University* 47 (10): 1555–1567. https://doi.org/10.13203/j.whugis20220412

Wang, Y., H. Z. Xu, and J. G. Zhan. 2001. "High-Resolution Seabed Topography of China Sea and Its Adjacent Seas." *Chinese Science Bulletin* 46 (11): 956–960. https://doi.org/10.3321/j.issn:0023-074X.2001.11.018

Watts, A. B. 1979. "On Geoid Heights Derived from Geos 3 Altimeter Data and Flexure of the Lithosphere along the Hawaiian-Emperor Seamount Chain." *Journal of Geophysical Research: Solid Earth* 84 (B8): 3817–3826. https://doi.org/10.1029/JB084iB08p03817

Yang, J. J., C. Jekeli, and L. T. Liu. 2018. "Seafloor Topography Estimation from Gravity Gradients Using Simulat ed Annealing." *Journal of Geophysical Research: Solid Earth* 123 (8): 6958–6975. https://doi.org/10.1029/2018JB015883